Cellular and Molecular Life Sciences (2019) 76:1987–2002
https://doi.org/10.1007/s00018-019-03030-7

ORIGINAL ARTICLE

Tight junction proteins at the blood–brain barrier: far more than claudin-5

Philipp Berndt[1] · Lars Winkler[1] · Jimmi Cording[1] · Olga Breitkreuz-Korff[1] · André Rex[2] · Sophie Dithmer[1] · Valentina Rausch[1] · Rosel Blasig[1] · Matthias Richter[3] · Anje Sporbert[3] · Hartwig Wolburg[4] · Ingolf E. Blasig[1] · Reiner F. Haseloff[1]

Received: 12 September 2018 / Revised: 15 January 2019 / Accepted: 28 January 2019 / Published online: 7 February 2019

Abstract

At the blood–brain barrier (BBB), claudin (Cldn)-5 is thought to be the dominant tight junction (TJ) protein, with minor contributions from Cldn3 and -12, and occludin. However, the BBB appears ultrastructurally normal in Cldn5 knock-out mice, suggesting that further Cldns and/or TJ-associated marvel proteins (TAMPs) are involved. Microdissected human and murine brain capillaries, quickly frozen to recapitulate the in vivo situation, showed high transcript expression of Cldn5, -11, -12, and -25, and occludin, but also abundant levels of Cldn1 and -27 in man. Protein levels were quantified by a novel epitope dilution assay and confirmed the respective mRNA data. In contrast to the in vivo situation, Cldn5 dominates BBB expression in vitro, since all other TJ proteins are at comparably low levels or are not expressed. Cldn11 was highly abundant in vivo and contributed to paracellular tightness by homophilic oligomerization, but almost disappeared in vitro. Cldn25, also found at high levels, neither tightened the paracellular barrier nor interconnected opposing cells, but contributed to proper TJ strand morphology. Pathological conditions (in vivo ischemia and in vitro hypoxia) down-regulated Cldn1, -3, and -12, and occludin in cerebral capillaries, which was paralleled by up-regulation of Cldn5 after middle cerebral artery occlusion in rats. Cldn1 expression increased after Cldn5 knock-down. In conclusion, this complete Cldn/TAMP profile demonstrates the presence of up to a dozen TJ proteins in brain capillaries. Mouse and human share a similar and complex TJ profile in vivo, but this complexity is widely lost under in vitro conditions.

Keywords Brain endothelium · Ischemia · Protein–protein interaction · Laser capture microdissection · Neurovasculature

Philipp Berndt and Lars Winkler contributed equally.

Electronic supplementary material The online version of this article (https://doi.org/10.1007/s00018-019-03030-7) contains supplementary material, which is available to authorized users.

✉ Lars Winkler
winkler@fmp-berlin.de

✉ Reiner F. Haseloff
haseloff@fmp-berlin.de

[1] Leibniz-Forschungsinstitut für Molekulare Pharmakologie, Robert-Rössle-Str. 10, 13125 Berlin, Germany

[2] Department of Experimental Neurology, Charité-Universitätsmedizin Berlin, Charitéplatz 1, 10117 Berlin, Germany

[3] Max-Delbrück-Centrum für Molekulare Medizin, Robert-Rössle-Str. 10, 13125 Berlin, Germany

[4] Institut für Pathologie und Neuropathologie, Universität Tübingen, Liebermeisterstraße 8, 72076 Tübingen, Germany

Abbreviations

BBB	Blood–brain barrier
BSA	Bovine serum albumin
CFP	Cyan fluorescent protein
Cldn	Claudin
CRFR	Corticotrophin-releasing factor receptor
DMEM	Dulbecco's modified Eagle's medium
EDTA	Ethylenediaminetetraacetic acid
FCS	Fetal calf serum
FRET	Fluorescence resonance energy transfer
HB-EGF	Heparin-binding epidermal growth factor-like growth factor
HEK	Human embryonic kidney
MBP	Maltose-binding protein
MCAO	Middle cerebral artery occlusion
MDCK	Madin–Darby canine kidney cells
MRI	Magnetic resonance imaging
Ocln	Occludin
PBS	Phosphate buffered saline

PEI	Polyethylenimine
qRT-PCR	Quantitative real-time polymerase chain reaction
RCA1	*Ricinus communis* agglutinin
SDS-PAGE	Sodium dodecyl sulfate polyacryl gel electrophoresis
TAMP	Tight junction-associated Marvel protein
TER	Transcellular electrical resistance
TJ	Tight junction
TX-100	Triton X-100
VEGF	Vascular endothelial growth factor
YFP	Yellow fluorescent protein

Introduction

The blood–brain barrier is an extremely fine-tuned biological interface—a highly restrictive barrier equipped with a multitude of transporters for brain nutrients. Claudins (Cldns) are the major component that establishes paracellular tightness between neighboring endothelial and epithelial cells [1, 2]. 27 members of this family have been described [3, 4]. Clnds build the backbone of tight junctions (TJs), forming an intramembranous network of strands between adhering plasma membranes. In these strands, most Cldns and TJ-associated marvel proteins (TAMPs: occludin (Ocln), tricellulin, marvelD3) heterophilically *cis*-associate along membranes [5] and *trans*-oligomerize between plasma membranes of opposing cells [6]. The varying barrier properties depend on the combination of tightening and pore-forming Cldns within the TJ strands [7]. Cldn composition and their arrangement within TJ strands are regulated in development and disease [8, 9].

The TJs of the blood–brain barrier (BBB) are among the most restrictive sealing elements throughout the organism and are formed between brain capillary endothelial cells [10]. This restriction protects the brain from both harmful substances and the effects of substrate fluctuations in blood, and maintains brain homeostasis. Cldn5 is thought to be the main TJ protein at the BBB [11]. Cldn5 knock-out mice exhibit increased BBB permeability for molecules < 800 Da; alterations in the morphology of the TJs have not been observed [12]. Although Cldn12 is certainly expressed [12], it does not form TJ strands, and it is unclear whether it is incorporated into existing strands, as neither homo- nor heterophilic interactions have been found [6]. In comparison with Cldn5, other tightening Cldns, such as Cldn1 or -3, are rather weakly expressed at the BBB [13–15]. Cldn11 transcript expression was reported in primary brain endothelial cells [16], and Cldn11 and Cldn5 protein, but no other claudins, have been identified in brain endothelial cells and capillaries very recently [17]. Thus, the question arises as to whether further TJ proteins incorporate into TJs of the BBB and whether Cldn5 deficiency is compensated by other TJ proteins.

An interplay between TJ proteins is a prerequisite for the regulation of barrier permeability and for compensatory mechanisms, but little is known about this. In endothelial cells, cadherin-5 controls Cldn5 by triggering transcriptional repression via FoxO1 and β-catenin [18]. However, β-catenin also activates the transcription of Cldn1 [19] and Cldn3 [20]. Ocln is highly expressed at the BBB and is controlled by different pathways. Multiple kinases and phosphatases have been identified to target Ocln, in particular in the C-terminal region [21]. In the endothelium of the blood–retinal barrier, vascular endothelial growth factor (VEGF)-dependent signal transduction involves conventional protein kinase C beta and atypical protein kinase C [22]. VEGF-mediated phosphorylation of Ocln at Ser490 increases its cytoplasmic localization [23]; concomitant redistribution of Cldn5 is in line with *cis*-interactions between Ocln and different Cldn variants [5].

In cerebral pathologies, TJ protein expression is modified and BBB tightness is affected. For example, disruption of the BBB is observed in neurological disorders such as multiple sclerosis, stroke, Alzheimer's disease, epilepsy, and traumatic brain injuries [24]. Cldn5, Ocln and cadherin-5 levels are decreased within the first hours of ischemia [25, 26]. β-Catenin is degraded during focal cerebral ischemia [27]. After hypoxia, Cldn1 is up-regulated in mouse brain endothelial cells [28], whereas levels of Cldn3 and Cldn5 in rat brains are decreased following ischemia (unilateral carotid artery ligation) [29]. Ocln plays a key role in response to redox changes and acts as a redox sensor and regulator at the TJs [30, 31]. Under the reducing conditions caused by hypoxia or ischemia, occludin is redistributed from the TJs to the cytosol, and the paracellular barrier is weakened [32, 30]. Intracellularly, occludin acts as an oxidase [33], thereby counterbalancing alterations in the redox status of the cells.

The function of the TJs largely depends on the molecular composition and stoichiometry of its constituents. In this respect, quantitative data are sparse and restricted to rodents and do not consider recent developments, such as the discovery of Cldn-25, -26 and -27, which localize to TJs after exogenous expression in epithelial cell lines [4].

Thus, the objectives of the present investigation are as follows: (1) to perform comprehensive identification and quantification of tetraspanning TJ transcripts/proteins at the BBB of human and mouse in vivo and in vitro, (2) to characterize the influence of pathological conditions on TJ protein expression and localization and finally, (3) to gain insight into the influence of Cldn deficiency on other TJ proteins. We have identified new members of the Cldn family at the BBB, with different abundance in man and mice in vivo and in vitro; they may also compensate for each other

under redox stress or after knock-down. Our data provide an explanation for the differences in barrier tightness between cellular and animal BBB models.

Experimental procedures

Materials

Cldn nomenclature was used as described [4]. The antibodies such as rabbit anti-Cldn1 (51-9000), rabbit anti-Cldn3 (34-1700), rabbit anti-Cldn4 (36-4800), mouse anti-Cldn5 (1548773A), rabbit anti-Cldn5 (QE215213), rabbit anti-Cldn11 (36-4500), rabbit anti-Cldn15 (389200), rabbit anti-Cldn25 (PA-25733), mouse anti-Ocln (33-1500) and horseradish peroxidase (HRP)-conjugated antibody were from Thermo Fisher Scientific (Waltham, USA). Mouse anti-β-actin (CP01) was from Merck Millipore (Darmstadt, Germany), rabbit anti-Cldn12 (JP18801) from IBL International (Hamburg, Germany), rabbit anti-Cldn20 (117678-1-Ab) from Proteintech (Rosemont, USA), rat anti-Zo1 (LSC124822) from Biozol Diagnostica (Eching, Germany) and mouse anti-NeuF (ab24574) from Abcam (Cambridge, UK).

Brain samples

Human cortices taken during autopsy and frozen 1–3 h post-mortem (Caucasian: two male 46 and 54 years, and two female 31 and 54 years, died in accidents) were purchased from AMS Biotechnology (Abingdon, UK) and ethically approved by the Western Institutional Review Board (Puyallup, USA; Protocol # CU-M-01142014-C). C57BL/6N mice were housed under standard conditions with a 12-h light–dark cycle, food and water ad libitum. All experiments were performed according to the guidelines for care and use of laboratory animals of the German Animal Welfare Act and approved by the local ethics committee (LaGeSo Berlin; T0457/09 and G0030/13).

Cerebral ischemia and capillary dissection

Filamentous middle cerebral artery occlusion (MCAO) was performed as described [34]. In brief, mice were anesthetized with 1% isofluorane in 70% N_2O and 30% O_2 using a vaporizer. Left MCA was occluded with an 8.0 nylon monofilament coated with a silicone resin/hardener mixture. Filaments were withdrawn after 30 or 60 min of ischemia to allow reperfusion for 48 h and 3 h, respectively. Magnetic resonance imaging (MRI) was accomplished to determine the infarct localization and size. After 3 h of reperfusion, the imaging was obtained by diffusion-weighted MRI. T_2-weighted imaging was performed after 48 h of reperfusion. Mice were sacrificed, brains were prepared, embedded in TissueTek (AMS Biotechnology, Abingdon, UK) and immediately frozen on dry ice in 2-methylbutane for 10 min. For laser capture microdissection, frozen brain sections (8 µm) were placed on Zeiss Membrane Slides 1.0 PEN (Jena, Germany). After 10 min of methanol fixation (− 20 °C), slides were washed with ddH_2O and stained with fluorescein-labeled *Ricinus communis* agglutinin (RCA1) DyLight594 (Vector Laboratories, Burlingame, USA) for 2 min (1:20 in ddH_2O) to visualize brain capillaries [35]. Additional washing (twice) was followed by consecutive dehydration steps (1 min 70%, 1 min 90%, 3 min 96%, 5 min 100% ethanol). The microvessels were dissected using a PALM MicroBeam (Zeiss) by following a procedure optimized with respect to optical resolution and speed. Applying the laser cut function "LineAutoLPC", the tissue was cut along the vessels and instantaneously catapulted in a contact-free mode into opaque Adhesive Caps 500 (Zeiss). Targets were drawn using a 10×/0.1 dry objective, and a LD 20×/0.2 dry objective was applied for cutting/catapulting. The cutting precision of this procedure was about 2.5 µm and the diameter of the resulting defocused LPC shot was approx. 3.5 µm. 500–1000 capillaries were cut per session.

In vitro brain capillary preparation and hypoxia

Mouse brain capillaries were isolated from four cortices of 8- to 20-week-old C57BL/6N mice of either sex [36] by homogenization in Dulbecco's modified Eagle's medium (DMEM, 4.5 g/l glucose; Life Technologies, Darmstadt, Germany) with a Dounce tissue grinder (Wheaton, Millville, USA) on ice. Myelin was removed by adding dextran (60–70 kDa, 16% (w/v) final concentration; Sigma-Aldrich, Taufkirchen, Germany) and centrifugation (15 min, 4500×*g*, 4 °C). The resuspended pellet was filtered (40-µm nylon mesh, Merck Millipore). The remaining capillaries were rinsed off with DMEM and 1% (v/v) fetal calf serum (FCS; Life Technologies). For normoxia/hypoxia, freshly purified capillaries were resuspended in 1.5 ml DMEM containing 10% FCS and incubated at 37 °C for 3 h [37] normoxically (5% CO_2/95% air) or hypoxically (< 0.3% O_2; anaerobic workstation Concept Plus; IUL Instruments/Russkin Technology, Bridgend, UK used according to the manufacturer's instructions).

Cell cultures and transfection

Primary mouse brain endothelial cells were obtained from purified capillaries by adding dispase (1.1 g/l) and collagenase (0.5 g/l) in 1 ml DMEM (4.5 g/l glucose) containing 2% (v/v) FCS and 1% (v/v) penicillin (100 U)/streptomycin (100 g/l). After 1 h at 37 °C, digested capillaries were centrifuged (250×*g*), resuspended in DMEM with 20% (v/v) FCS

and 1% penicillin/streptomycin supplemented with 0.5% (v/v) mouse serum and 1 ng/ml basic fibroblast growth factor (Life Technologies), and transferred to collagen-coated 24-well plates (Techno Plastic Products, Trasadingen, Switzerland) kept at 37 °C and 5% CO_2. The mouse brain endothelial cell line bEND.3 [38] was cultured in DMEM (4.5 g/l glucose, 10% FCS, 1% penicillin/streptomycin) at 37 °C and 5% CO_2; the cell lines human embryonic kidney (HEK)-293 and MDCK-II were maintained in DMEM (1 g/l glucose, 10% FCS, 1% penicillin/streptomycin) at 37 °C and 10% CO_2.

Transfections were performed with polyethylenimine (PEI; Polysciences, Warrington, USA) according to the supplier's recommendations; cells were used for experiments at 48 h post-transfection [5].

For knock-down of Cldn5 and -25, lentiviral particles were generated with the expression vector pLKO.1puro containing the respective shRNA (Cldn5, NM_013805.2-774s1c1; Cldn25, NM_171826.1-347s1c1; non-mammalian control, SHC002). Using the transfection method described above, viral particles were produced in HEK-293T cells (kindly provided by M. Krauss, Berlin). Cells were transfected with 0.17 µg/cm^2 pLKO.1 puro/shRNA (Sigma-Aldrich), psPAX2 (virus packaging) and pMD2.G (virus envelope) plasmids (kindly provided by M. Lehmann, Berlin) in a ratio of 2:2:1 in PEI (bEnd.3 medium, 37 °C, 5% CO_2, 96 h). After 48 h, the medium was exchanged and supplemented with 1 µg/ml puromycin to select knock-down cells. The medium was harvested, centrifuged (600×*g*), and the supernatant was filtered (Steriflip filter unit, 0.45 µm). The filtrate was concentrated (Amicon Ultra-15, 100 K; Merck Millipore) (3000×*g*, 60 min) and added to 25% confluent bEnd.3 cultures. The knock-down efficiency was determined by qRT-PCR.

Quantitative real-time polymerase chain reaction (qRT-PCR)

RNA was extracted by GeneMATRIX Universal RNA purification kit (EURx, Gdansk, Poland), and the cDNA was synthesized with Maxima First Strand cDNA synthesis kit (Thermo Fisher Scientific). The qRT-PCR was performed with a StepOne RT-PCR system, 48/96 well (Life Technologies) using the Luminaris Color HiGreen high ROX qPCR master mix (Thermo Fisher Scientific) as recommended by the manufacturer. Primer pairs (BioTeZ, Berlin, Germany, cf. Tab. S2) were designed according to http://primer3plus.com [39] and proved for specificity. The cycle-thresholds (Ct) were normalized to those of β-actin (Actb) or 28S ribosomal RNA by calculating $\Delta Ct = (Ct_{\text{target protein}} - Ct_{\text{Actb or Rn28S}})$. For comparing expression between two groups, relative values were calculated by $2^{\Delta\Delta Ct}$, where $\Delta\Delta Ct = \Delta Ct_B - \Delta Ct_A$. Experimental detection limits of $2^{\Delta Ct}$ values (termed absolute values) were 3.37×10^{-5} (laser microdissected capillaries), 2.03×10^{-5} (in vitro capillary preparations), 5.75×10^{-7} (primary bEnd), and 8.83×10^{-7} (bEnd.3).

Expression constructs

Mouse Cldn5–YFP (yellow fluorescent protein), human YFP– and CFP–(cyan fluorescent protein)Cldn11, human corticotrophin-releasing factor receptor (CRFR)-1–YFP and –CFP as well as CFP–Ocln, and MBP(maltose-binding protein)–$Ocln_{406–521}$ from mouse were as described earlier [5, 6, 40]. YFP–Cldn11 and -25 were amplified from mouse brain cDNA using PCR primers (cf. Tab. S2) and inserted into pEYFP-C1 using the restriction sites *Eco*R1 and *Sal*1, and *Hin*dIII and *Sal*1, respectively.

For the epitope dilution assay, MBP-fusion constructs with antibody recognition epitopes of mouse (m)Cldns 1, 4, 5, 11, 12 and 25 were generated. Sequences were cloned via *Bam*HI and *Sal*I sites (underlined in Tab. S2) into pMAL-c2X (NEB, Schwalbach, Germany) after cDNA amplification using primers (cf. Tab. S2) and respective Cldn–cDNA from mouse tissue as a template.

Epitope dilution assay

MBP-fusion proteins containing the epitopes for the antibodies used in this assay were expressed in *E. coli* BL21 after induction (1 mM isopropyl β-D-1-thiogalactopyranoside, 3 h, 37 °C) [41]. Cells were spun (3220×*g*, 15 min, 4 °C) and lysed after resuspension in 20 mM Tris/HCl pH 7.4, 0.2 M NaCl, and 1 mM ethylenediaminetetraacetic acid (EDTA) by homogenization (EmulsiFlex-C3; Avestin Europe, Mannheim, Germany). Lysate and the resulting supernatant were centrifuged (20,000×*g*, 4 °C, 15 min; 60,000×*g*, 4°C, 1 h). MBP constructs were purified via amylose resin (New England Biolabs, Frankfurt, Germany) according to the manufacturer's instructions.

Purified capillary pellets were suspended in extraction buffer: PBS (phosphate buffered saline, Biochrom), 1% TX-100 (Sigma-Aldrich), and 10% complete protease inhibitor cocktail (Roche, Basel, Switzerland) on ice for 20 min. The lysate was centrifuged (13,000×*g*, 1 min) and the supernatant (TX-100-soluble fraction) was mixed 1:10 with lysis solubilization buffer: 50 mM Tris/HCl pH 8.8, 5 mM EDTA, 1% sodium dodecyl sulfate, (SDS; Sigma-Aldrich). The pellet (TX-100-insoluble fraction) was treated with benzonase (Merck Millipore) in 5 µl 50 mM Tris/HCl pH 8.8 and 2 mM $MgCl_2$ at 37 °C for 10 min. 16.6 µl solubilization buffer was added, the benzonase was heat inactivated (95 °C, 3 min), and 11.7 µl extraction buffer was added to adjust the volume.

Total protein concentrations of capillary lysate fractions were detected by a Pierce BCA Protein Assay Kit (ThermoFisher Scientific) in a microplate detection system

(Safire; Tecan, Männedorf, Switzerland). MBP-fusion protein concentrations were determined using NanoDrop 2000c (Thermo Fisher Scientific; $\lambda_{exc} = 280$ nm, extinction coefficient calculated by ProtParam, www.expasy.org). Dilution series of the epitopes fused to MBP were loaded together with the capillary lysate for SDS polyacryl gel electrophoresis (SDS-PAGE) (Fig. 2a). SDS-PAGE and western blotting were performed as described previously [42] using the respective Cldn and Ocln antibodies. Immuno-reactive bands were detected using Lumi-Imager F1T transilluminator (Boehringer-Mannheim, Germany). ImageJ 1.48v (National Institutes of Health, Bethesda, USA) was applied for densitometric analyses, and calibration curves were generated to determine absolute Cldn and Ocln quantities in capillary lysates.

Immunohistochemistry and immunofluorescence

Cerebral cortices were cut (8 µm, cryostat CM 3000; Leica, Wetzlar, Germany) and fixed with methanol on glass slides (10 min, − 20 °C). Brain sections were blocked with 2% bovine serum albumin (BSA) for 30 min and incubated with the primary antibody (18 h, 4 °C). The immunoreactivity of primary antibodies was visualized with secondary anti-mouse, -rabbit and -rat AlexaFlour488 or -555 conjugated antibodies. If applicable, fluorescein-labeled RCA1 was added afterwards for 2 min. Tissue was mounted with Roti-Mount FluorCare DAPI (4′,6-diamidino-2-phenylindole for nuclear staining; Roth, Karlsruhe, Germany). For immunocytochemistry, bEND.3 cells were grown to confluency on coverslips (Menzel, Braunschweig, Germany) coated with rat tail collagen (Roche) and fixed with acetone as described previously [41]. Tissues and cells were examined by Zeiss LSM 780 with 64 ×/1.40 oil objective.

trans-Interaction, *cis*-interaction, and membrane mobility

HEK-293 cells grown to confluency were imaged using LSM 510 META UV and Plan-Neofluar 100x/1.3 NA oil immersion objective (Zeiss) [5]. Plasma membranes were visualized by trypan blue (0.05%; Sigma-Aldrich) in Hanks' balanced salt solution, pH 7.5. For *trans*-interactions, the enrichment factor EF was detected. Half the fluorescence intensity (I) of a YFP- or CFP-tagged protein at cell–cell contacts between two transfected cells was divided by YFP or CFP fluorescence at contacts between expressing and non-expressing cells ($EF = I_{contact}/2I_{no\ contact}$) [43]. For *cis*-interactions along the membrane of a cell–cell contact, fluorescence resonance energy transfer (FRET) after acceptor photobleaching was determined in HEK-293 cells co-transfected with YFP-/CFP-labeled Cldns [43]. Cldn5–CFP/corticotrophin-releasing factor receptor-1–YFP served as negative control. For Cldn11 membrane mobility, fluorescence recovery after photobleaching (FRAP) was measured using Zeiss LSM 710 with Plan-Apochromat 63 ×/1.40 Oil DIC M27 objective ($\lambda_{exc} = 405$-nm intensity set to 2.0%, filters, $\lambda = 415$–551 nm). Images were collected each 60 s until steady-state fluorescence was reached. The mean fluorescence of whole-cell background and bleached bicellular TJ regions was quantified over time.

Transcellular electrical resistance (TER) measurements

bEND.3 cells were seeded into poly-L-cysteine-coated (10 mM, Sigma-Aldrich) eight-well electrode arrays (8W10E+, Ibidi GmbH, Planegg, Germany) of the electric cell-substrate impedance sensing device ECIS 1600R (Applied BioPhysics, Troy, USA). The impedance was measured in real time at 4 kHz. The TER was calculated after reaching constant impedance values. Confluent MDCK-II monolayers were grown on rat tail collagen (Roche)-coated filters (0.4 µm pore size, Millicell-CM; Merck-Millipore). The TER was measured manually using a EVOM voltohmmeter (World Precision Instruments, Sarasota, USA) at 37 °C.

Freeze-fracture electron microscopy

Confluent bEND.3 and 85% confluent HEK-293 cells were washed with PBS (with Ca^{2+}/Mg^{2+}) and fixed with 2.5% glutaraldehyde (electron microscopy grade; Sigma-Aldrich) for 2 h at room temperature. Afterwards, the cells were washed twice and processed for freeze-fracturing as described [31].

Statistics

Any sample sizes are given as discrete numbers. Data analysis and assembly of graphs were achieved by employing GraphPad Prism 5.04 and Microsoft Excel 2010. For statistical analysis, Mann–Whitney or Kruskal–Wallis test was applied. If not stated otherwise, data are given as mean ± SD (*$p < 0.05$; **$p < 0.01$; ***$p < 0.001$).

Results

Diversity of tight junction proteins at the blood–brain barrier

The expression of TJ protein transcripts was analyzed by qRT-PCR in human and mouse cortical capillaries (laser capture microdissected from frozen tissue), in purified capillary preparations from mouse cortex, in primary mouse brain endothelial cells and in the cell line bEND.3 (Fig. 1).

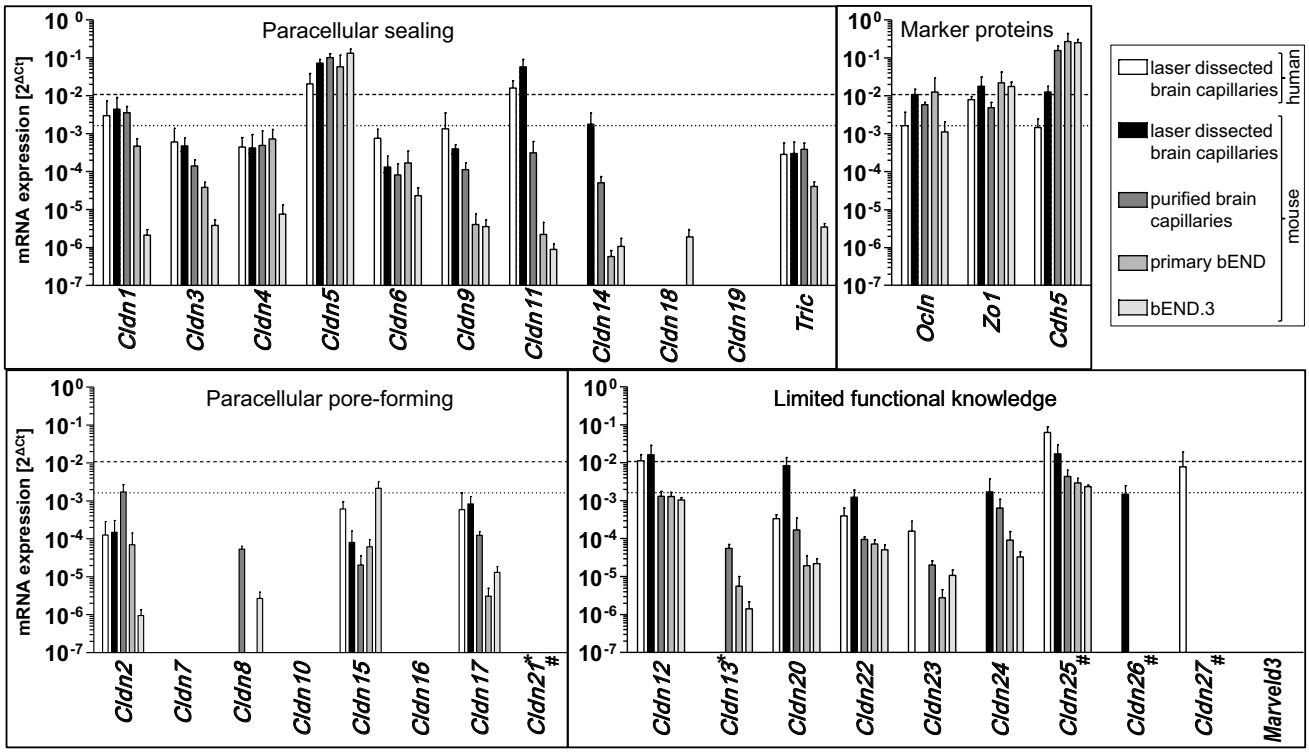

Fig. 1 Diversity of mRNA expression of tight junction proteins in human and murine brain endothelium. Transcript levels in laser-dissected human and murine brain capillaries, purified murine brain capillaries, primary murine brain capillary endothelial cells and bEND.3, an endothelial cell line of the murine cerebral cortex. mRNA expression normalized to that of β-actin ($\Delta Ct = Ct_{target} - Ct_{actin}$). *Cldn* claudin, *Tric* tricellulin, *Ocln* occludin, *Zo1 Zonula occludens* protein 1, *Cdh5* cadherin-5, *Ct* cycle threshold. Dotted/dashed line, Ocln expression in laser microdissected human/mouse brain capillaries (used as a benchmark of tight junction protein abundance); missing columns, mRNA not detectable (detection limit for $2^{\Delta Ct}$ is 5.75×10^{-7} in primary murine brain capillary endothelial cells). *Cldn13 (human) and Cldn21 (mouse), not determined; #synonyms: human Cldn21, putative Cldn25; Cldn25, Cldnd1; Cldn26, Tmem114; Cldn27, Tmem235

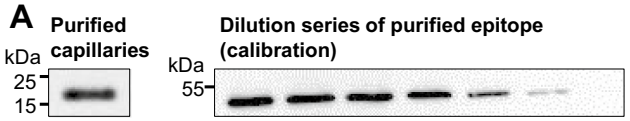

B

Molality in purified brain capillaries [fmol/µg]

	Triton X-100 insoluble	Triton X-100 soluble
CLDN1	9.7 ± 6.9	4.8 ± 8.2
CLDN4	1.5 ± 2.9	3.4 ± 6.2
CLDN5	113.6 ± 74.0	395.3 ± 291.9
CLDN11	6.3 ± 4.3	1.7 ± 1.2
CLDN12	n.d.	4.3 ± 3.5
CLDN25	97.8 ± 112.7	n.d.
OCLN	26.5 ± 8.6	9.6 ± 4.3

Fig. 2 Protein levels of tight junction proteins in purified brain capillaries (fmol/µg total protein). **a** Representative images of western blots to quantify the TJ protein concentration via a dilution series of the purified Cldn epitope recognized by the respective antibody. The endogenous protein in purified brain capillaries is shown on the left. The dilution series was realized by recombinant MBP-tagged epitopes. **b** Protein concentrations given for Triton X-100 (TX-100)-insoluble and -soluble fraction. *n.d.* not detectable; mean ± SD; $n \geq 4$

Junctional marker proteins, such as *Zonula occludens* protein 1 (Zo1), cadherin-5 or Ocln, showed expression levels as expected from previously published data [13, 14]. In general, the results indicate the existence of many more Cldns than those yet described for the BBB [2].

In human capillaries, mRNA transcripts of Cldn1, -5, -11, -12, -25 and -27 were found in higher abundance than the mRNA of the TJ marker Ocln (which we consider as a benchmark of TJ protein expression). Numerous gene products (Cldn3, -4, -6, -9, -15, -17, -20, and -22, and Tric) were detected within one order of magnitude of Ocln, whereas other claudins and TAMPs were not detectable or made only a minor contribution to the tight junction transcriptome (cf. Table S1 for absolute mRNA values and Fig. S1 for a graphical transformation of their proportions). Levels of Cldn7, -8, -10, -13, -16, -18, -19, and -21 and MarvelD3 were consistently negligible.

In capillaries microdissected from mice, mRNA levels of Cldn5, -11, -12 and -25 were higher than those of occludin. Expression values of Cldn1, -14, -20, -22, -24 and -26 were found within one order of magnitude of occludin.

Only Cldn5 levels exceeded those of Ocln in purified capillary preparations and primary endothelial cells; Cldn12 and -25 (both preparations), and Cldn1, -2, and -24 in capillaries exhibited mRNA levels within the interval of one order of magnitude. Of the different preparations, bEND.3 cells showed the lowest values for the Ocln transcript and, with a few exceptions, also the lowest mRNA levels for the other genes. However, Cldn5 was the dominant species in this cell line, with some expression levels also being greater than (Cldn15 and -25) or close to Ocln (Cldn12). In general, the decrease in the complexity of the TJ transcript follows the decrease in complexity of the model.

Tight junction protein levels in brain capillaries as demonstrated by a new protein quantification assay

The parallelism of data obtained for TJ mRNA and protein amounts was analyzed by application of a new antibody epitope dilution assay based on recombinantly expressed and purified epitopes of Cldns and Ocln recognized by the respective antibodies. This approach allowed us to determine the Cldn/TAMP content in lysates of purified mouse brain capillaries, as shown for Cldn5 (Fig. 2a). Ranking of the protein levels (Cldn5 $\gg$ Cldn25, Ocln, Cldn1 > Cldn11, -4, -12) is broadly consistent with the mRNA data (Fig. 2b). Cldns 4 and 5 were enriched in the TX-100-soluble fraction, while Cldn1 and -11, and Ocln were more abundant in the TX-100-insoluble fraction. Cldn12 was only detectable in the TX-100-soluble fraction. In contrast, Cldn25 was exclusively found in the insoluble fraction.

Novel blood–brain barrier claudins 4, 11, 20 and 25 localize to the tight junction area

Immunofluorescence staining of human brain sections was performed to investigate the relevance of the identified Cldns for TJ formation (Fig. 3). As Zo1 co-localized perfectly with Ocln (upper left panel in Fig. 3), it was used as a surrogate marker. Brain capillaries, the main cellular BBB constituent, were depicted by the endothelium-specific lectin RCA1 [35]. Cldns 1, -3, -4, -5, -11, -20 and -25 co-localized with Zo1. However, the anti-Cldn25 antibody additionally displayed faint staining outside the endothelium (Fig. 3, bottom right).

As already described [44], Cldn11 also localized to oligodendrocytes wrapped around axons of neurons (Fig. 3, 3rd panel right). However, cortex tissue sections demonstrated that Cldn11 was predominantly localized in blood vessels (Fig. 3). Data obtained for Cldns 1, -4, -5, and -11 in mouse samples (Fig. S2) correspond to those found in man.

Claudin-11 tightens cell barriers and only interacts homophilically in *cis* and *trans*

As Cldn11 was one of the most highly expressed TJ proteins of the BBB, more detailed characterization was conducted. Cldn11 was originally identified as oligodendrocyte-specific protein [45] and later assigned to the claudin protein family [46]. Oligodendrocytes form myelin sheaths around axons. Accordingly, Cldn11 was detected together with neurofilament, a neuronal marker (Fig. 4b). In human brain sections, partial overlap of Cldn11 with Cldn5 was observed in the TJs of capillaries, interrupted by areas of exclusive Cldn11 staining (Fig. 4a). A control experiment measured a ratio of 1.61 ± 0.88 of the mRNA levels in RCA-stained samples and in surrounding tissue. To analyze the interaction properties of Cldn11 in a TJ-free environment, Cldn11 was expressed in HEK-293 cells (Fig. 4d–g). Co-culture of HEK-293 cells mono-transfected with either CFP–Cldn11 or YFP–Cldn11 exhibited strong co-enrichment at cell–cell contacts, indicating remarkable homophilic *trans*-interaction (enrichment factor $E_F = 93$ according to Fig. 4d, compared to $E_F = 5$ for Cldn5 [6]). The homophilic *cis*-interaction along the plasma membrane was also stronger for Cldn11 than for Cldn5, as demonstrated by fluorescence resonance energy transfer (FRET) efficiency of $60.6 \pm 14.2\%$ (Fig. 4f) vs. $18.5 \pm 1.5\%$ for Cldn5 [41]. However, Cldn11 was incapable of undergoing heterophilic *cis*- and *trans*-interactions with Clnds 1-5, -12, -22, -24, and -25, Ocln or Tric (examples for Cldn5/Cldn11 given in Fig. 4e, g; FRET efficiencies ≈ 1). Accordingly, Cldn11 and -5 exhibit fragmented, alternating localization within the cell contact membrane in brain capillaries (Fig. 4a, b), after co-transfection in HEK-293 cells (Fig. 4g) or transfection into bEND.3 cells (Fig. 4c).

The strong homophilic interactions of Cldn11 point to tight immobilization at cell–cell contacts, and was substantiated by means of fluorescence recovery after photobleaching. In agreement with previous studies [6], Cldn5 exhibited a mobile fraction of $42.3 \pm 14.7\%$. Cldn11 was much less mobile at contacts ($8.5 \pm 6.4\%$), reflecting the strong homophilic *cis*- and *trans*-interactions (Fig. 4h). The sealing potential of Cldn11 was measured after stable transfection in Madin–Darby canine kidney cells (MDCK-II); we observed an increase in TER to $93.3 \pm 15.2\ \Omega\ cm^2$, compared to $71.1 \pm 8.0\ \Omega\ cm^2$ of control MDCK-II cells (Fig. 4i). This indicates that Cldn11 has a tightening function.

Despite its inability to undergo heterophilic association, Cldn11 was influenced by the TJ regulator Ocln. This effect was visualized in freeze-fracture electron microscopy by the cell contacts of TJ-free HEK-293 cells. Transfection of Cldn11 mainly caused a TJ strand network associated with the protoplasmic fracture face, and

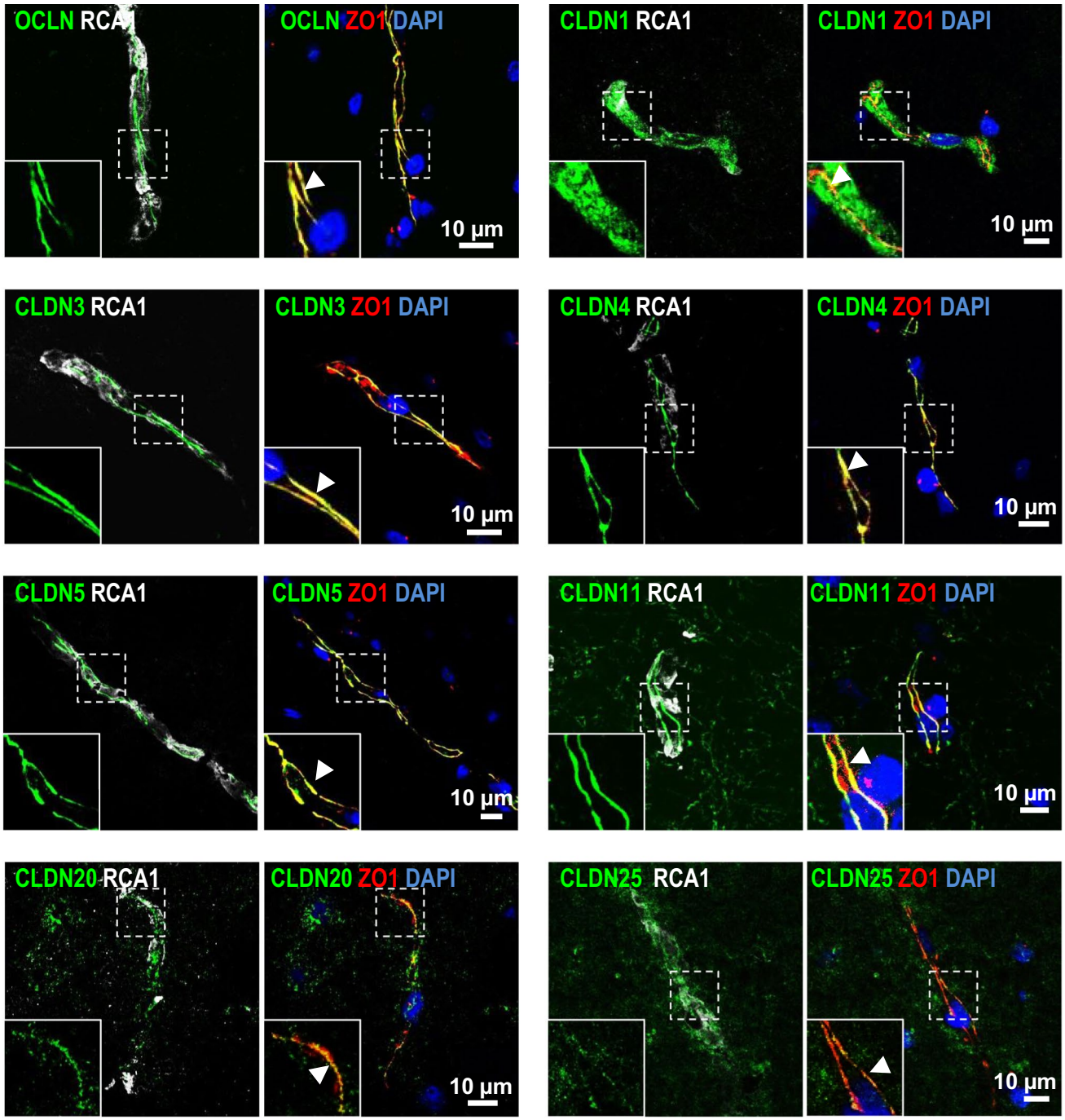

Fig. 3 Claudin (Cldn)-1, -3, -4, -5, -11, -20, and -25 and occludin (Ocln) co-localize to the tight junction (TJ) area of human brain capillaries. Immunofluorescence staining of human brain sections for TJ proteins (green). Microvessels were visualized by RCA1 (*Ricinus communis* agglutinin 1, white), an endothelial marker. The TJ marker Ocln exclusively localized to cell–cell contacts visualized by the junction marker Zo1 (*Zonula occludens* protein 1, red). Arrowheads indicate overlap of TJ proteins with Zo1 (yellow-orange); nuclei stained by DAPI (blue)

with a limited number of parallel strands and meshes of 200–300 nm in diameter. After co-transfection of Ocln, the parallelism increased, whereas the mesh size decreased (Fig. 4j).

Claudin-25, a further tight junction protein at the blood–brain barrier

Cldn25 exhibited similar abundance to Cldn12 in brain

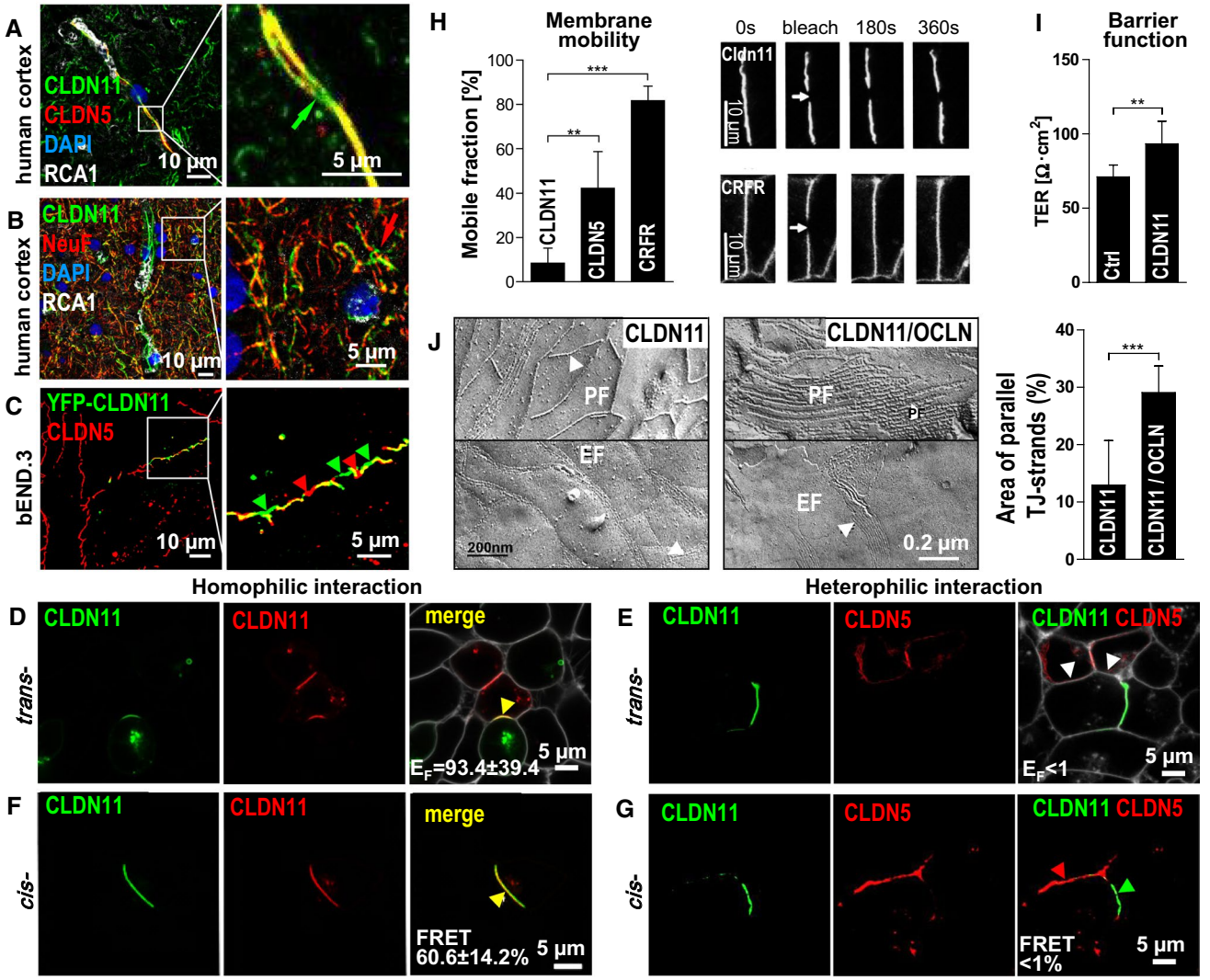

Fig. 4 Claudin(Cldn)-11 increases transcellular electrical resistance (TER) through homophilic but not heterophilic *cis*- and *trans*-interactions. In brain, Cldn11 localized in **a** capillaries (marker: RCA1) and in **b** oligodendrocytes ensheathing neuronal processes (marker: neurofilament, NeuF; red arrow). In capillary tight junctions (TJs), Cldn11 was traced with and without (green arrow) the cerebral TJ marker Cldn5. **c** After transfection in mouse brain endothelial cells (bEND.3), yellow fluorescent protein (YFP)–Cldn11 alternated with endogenous Cldn5 within TJs (red/green arrowhead). **d** Co-culture of cells mono-transfected with cyan fluorescent protein (CFP)–Cldn11 or YFP–Cldn11, plasma membrane of living cells visualized by trypan blue (white). Co-localization (yellow arrowhead) indicated strong homophilic *trans*-interaction quantified by the enrichment factor (E_F). **e** Living cells mono-transfected with CFP–Cldn11 or Cldn5–YFP showed no heterophilic *trans*-interaction (white arrowhead), $E_F < 1$; plasma membrane (white). Image representative for all other claudins tested. **f** Cells co-transfected with CFP/YFP–Cldn11 showing strong homophilic *cis*-interaction (yellow arrowhead) in cell contacts quantified by FRET (fluorescence resonance energy transfer). **g** No co-localization of CFP–Cldn11 and Cldn5–YFP in co-transfected cells, FRET efficiency < 1% as for all other claudins tested. **h** CFP–Cldn11 displayed much lower membrane mobility than CFP–Cldn5 or the negative control corticotropin releasing factor receptor (CRFR)–CFP, quantified in cells by fluorescence recovery after photobleaching. Kruskal–Wallis test; $n \geq 9$. **i** Transfection of CFP–Cldn11 in Madin–Darby canine kidney (MDCK-II) cells increased transcellular electrical resistance (TER) compared to non-transfected cells, Mann–Whitney test; $n \geq 9$. **j** Occludin (Ocln) modulated the TJ strands (arrowheads) of claudin-11 visualized by freeze-fracture electron microscopy of cells mono-transfected with CFP–Cldn11 (branched single strands) or co-transfected with CFP–Cldn11/YFP–Ocln (parallel strands). EF/PF, extracellular/protoplasmic fracture face; Mann–Whitney test, $n \geq 6$. In **d**–**h** and **j**, TJ-/Cldn-free HEK-293 cells were used. Mean ± SD; $*p < 0.05$; $**p < 0.01$; $***p < 0.001$

capillaries (Fig. 1). Its subcellular distribution was studied in more detail after transfection into HEK-293 cells: YFP–Cldn25 clearly localized to the plasma membrane, but was not enriched at cell–cell contacts of transfected cells (Fig. 5a). The contact enrichment factor for YFP–Cldn25-transfected HEK-293 cells or for co-cultured cells mono-transfected with YFP–Cldn25 and CFP–Cldn5 did not reveal enrichment, either for Cldn25/

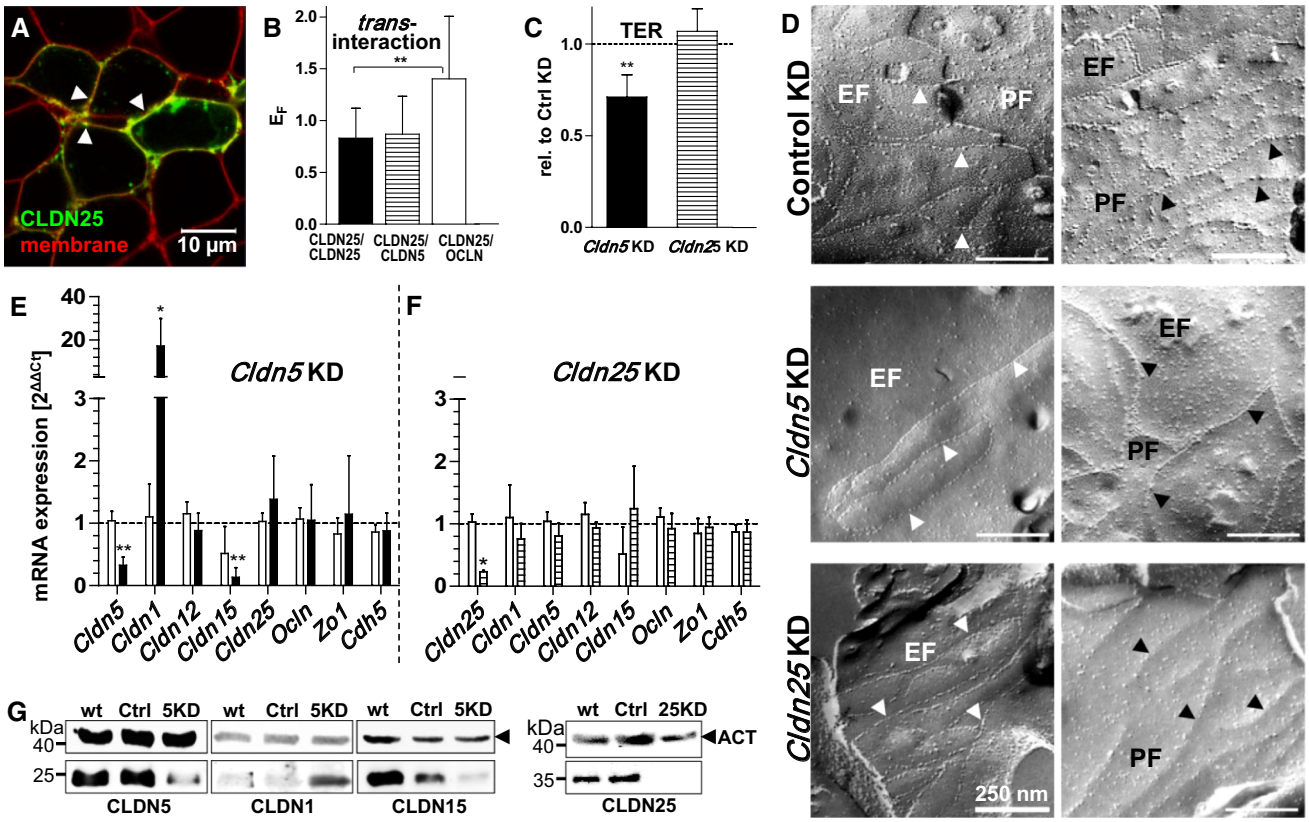

Fig. 5 Loss of claudin (Cldn)-25 and -5 compromises tight junction (TJ) strand morphology, whereas decrease in paracellular tightness and changes in TJ protein expression occur in Cldn5 knock-down (KD) only. **a** In living HEK (human embryonic kidney)-293 cells, transfected yellow fluorescent protein(YFP)–Cldn25 (green) localized at the plasma membrane (red, trypan blue) but **b** no homophilic *trans*-interaction of Cldn25 was found based on calculation of the enrichment factor (E_F) quantifying the fluorescence intensity at contacts (arrowheads in **a**) between transfected cells. However, E_F increased between YFP–Cldn25 and YFP–Ocln, suggesting heterophilic *trans*-interaction; Student's *t* test, $n \geq 8$. **c**–**g** experiments in bEND.3 (mouse brain endothelial cell line): **c** Cldn5 KD but not Cldn25 KD affected transendothelial electrical resistance (TER) compared to control (Ctrl, dashed line); Kruskal–Wallis test; $n \geq 8$. **d** Cldn5 KD weakened the TJ strand network on the extracellular (EF) and protoplasmic (PF) fracture face, i.e. enlarged and more round-shaped meshes. Cldn25 KD led to more unstructured strands and reduced mesh number on PF, i.e. less particles on the strands and larger meshes. **e** Cldn5 KD (black bars) but not **f** Cldn25 KD (striped bars) influenced the mRNA expression of other Cldn's mRNA compared to control KD (white bars), expression levels normalized to wild-type (wt) cells (dashed line). $\Delta\Delta Ct = (Ct_{target} - Ct_{actin})_{KD} - (Ct_{target} - Ct_{actin})_{wt}$; Ct, cycle threshold. Kruskal–Wallis test; $n \geq 4$. **g** Western blots of wt, Ctrl KD, Cldn5 KD (5KD), Cldn25 KD (25KD), loading control β-actin (ACT). Mean ± SD; $n \geq 4$; $^*p < 0.05$; $^{**}p < 0.01$

Cldn25 or for Cldn25/Cldn5. However, in co-cultures of YFP–Cldn25/CFP–Ocln, E_F increased by 68% compared to Cldn25/Cldn25 (Fig. 5b).

For further characterization, we silenced Cldn25 or Cldn5 in bEND.3 cells by a lentiviral approach. As expected, the Cldn5 knock-down cells showed a significant reduction in barrier tightness. For Cldn25, no change in TER was detected (Fig. 5c), but the TJ strand network was less accentuated. Larger and weaker P-face-associated meshes and a lower particle density were visualized by freeze-fracture electron microscopy. After knock-down of Cldn5, the meshes were larger and the number of strands was reduced. Moreover, the orientation of the strands was disturbed, especially at the E-face, but the P-face association was also diminished after Cldn5 suppression (Fig. 5d).

Transcriptional interdependency of claudin-1, -5 and -15

Knock-down of Cldn5 was found to alter mRNA expression of other TJ proteins (Fig. 5e)—which was not seen upon loss of Cldn25 (Fig. 5f). The level of Cldn1 was increased by approx. 17-fold, and the amount of Cldn15 decreased to approx. 1/8 after Cldn5 suppression (Fig. 5e, f). This effect was also reflected by the protein levels, as demonstrated by immunoblotting (Fig. 5g).

Ischemia up-regulates claudin-5 and -25, and down-regulates claudin-1, -3, and -12, and occludin

After a stroke, the BBB is known to be impaired, and this is accompanied by alterations in Cldn5 and Ocln [47]. Stroke-related experiments were performed to explore the implications of pathological conditions for other TJ proteins. After 60 min of MCAO in the mouse followed by 3 h of reperfusion, cortical mRNA expression of Cldn1, -3, -12 and Ocln decreased to 68, 24, 59 and 77%, respectively, compared to the contralateral control region. Ischemia-affected regions were identified via magnet resonance imaging, and respective capillaries were harvested by laser capture microdissection. Cldn5 (214%), Cldn25 (163%), Cldn11 and Cldn20 (by trend only) were up-regulated during post-ischemic reperfusion (Fig. 6a). An increase of 140% was observed for HB-EGF (heparin-binding epidermal growth factor-like growth factor), which is known to be up-regulated by ischemia and is suitable as an indicator of ischemic injury [48] (Fig. 6a). To study the aspect of oxygen depletion, a major pathogenic factor in ischemic disturbances, purified mouse brain capillaries were exposed to hypoxia in vitro for 3 h. The mRNA levels of Cldn1, -3, and -12, and Ocln were reduced to 20%, 37%, and 60%, and 69%, whereas Cldn11 tended to be increased (Fig. 6b), respectively. However, Cldn5 and -25 mRNA levels were not affected. Hypoxic conditions were verified by up-regulation of the endothelial hypoxia marker glucose transporter 1 [37] (Fig. 6b).

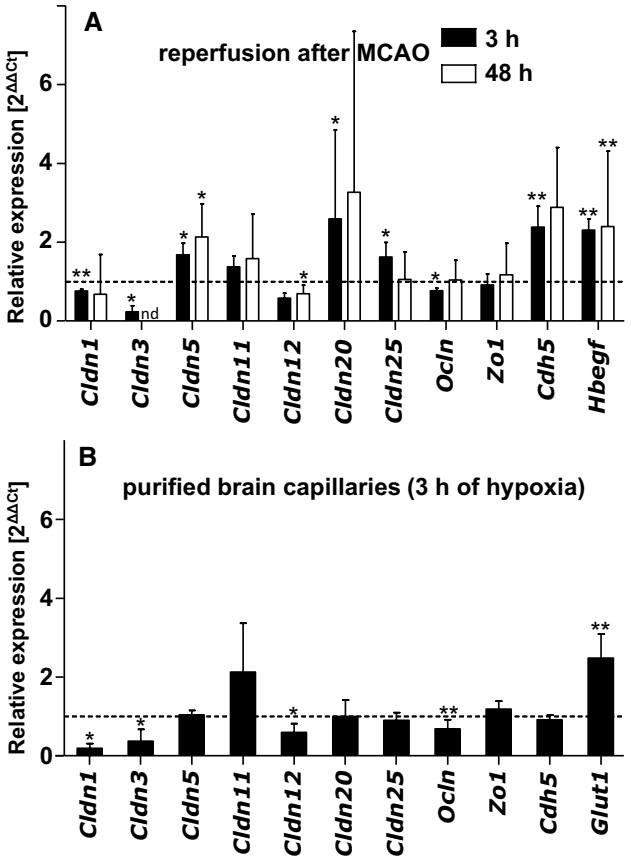

Fig. 6 In cerebral capillaries, mRNA expression of claudin(Cldn)-1, -3, and -12, and occludin (Ocln) is reduced under hypoxic conditions in vitro and under post-ischemic reperfusion in vivo, which in vivo is compensated by enhanced expression of Cldn- 5 and -25. **a** mRNA expression in laser-dissected mouse brain capillaries after middle cerebral artery occlusion (60 min or 30 min, corresponding reperfusion for 3 h or 48 h), normalized to the contralateral region (dashed line). $\Delta\Delta Ct = (Ct_{target} - Ct_{Rn28S})_{ipsilateral} - (Ct_{target} - Ct_{Rn28S})_{contralateral}$; Ct, cycle threshold. Heparin-binding epithelial growth factor-like growth factor (Hbegf) was used as indicator for ischemic dysfunction (nd, not detected). **b** mRNA expression in purified mouse brain capillaries exposed to 3 h of hypoxia; dashed line, expression levels under normoxic conditions. $\Delta\Delta Ct = (Ct_{target} - Ct_{actin})_{hypoxia} - (Ct_{target} - Ct_{actin})_{normoxia}$. Glucose transporter type 1 (Glut1) served as an indicator for hypoxic condition. Mean ± SD, $n \geq 4$, Mann–Whitney test; $^{*}p < 0.05$; $^{**}p < 0.01$. Rn28S, 28S ribosomal RNA; Zo1, *Zonula occludens* protein 1; Cdh5, cadherin-5. No other Cldn exhibited significant changes

Discussion

This study provides a complete profile of tetraspanning TJ proteins in human and mouse BBB in vivo and in vitro, and under pathological conditions. The results corroborate our hypothesis that not only Cldn3, -5, and -12, and Ocln [12, 49] but a larger number of other proteins establish the TJs of the BBB.

In contrast to in vitro BBB models, it turned out that Cldn5 mRNA in vivo is merely one of six other high abundant tetraspanning TJ protein transcripts. Amounts of mRNA of Cldns 11, -12, and -25, Ocln (human and mouse), and Cldns 1 and 27 (human) are in the same quantitative range within a species. Translated into the functional level, this suggests that a complex of complementary proteins (mainly claudins) operates the paracellular space of the BBB in vivo. This joint operation is lost in vitro where Cldn5 is dominant. Analogously to Cldn5 in the BBB, Cldn1, -9 and -11 could function as paracellular tightening proteins in epidermis [50], cochlea [51] and blood–testis barrier [52], respectively. The presence of additional TJ-forming Cldns in vivo can explain why TJs at the BBB of Cldn5-deficient mice are well developed [12]. On the other hand, the absence of several high abundant Cldns in vitro may also account for the relatively low tightness of in vitro BBB models [53].

Besides the aforementioned TJ proteins in capillaries microdissected from brain slices, substantial amounts of other claudin transcripts (nine in human, six in mouse) were found and these might also contribute to BBB function. Based on our data, in both species only Cldns 7, 10, 13, 16, 18, 19, 21, and 8 (human), 27 (mouse), and MarvelD3 have a negligible influence on brain microvasculature. The differences between the human and the mouse transcript are not

striking. Deviation of more than one order of magnitude in mRNA levels was found only for Cldns 9, 14, 20, 23, 24, 26 and 27.

The relevance of proteins at lower abundance can be illustrated for Cldn3: similar levels of Cldn3 were observed in cerebral capillaries [15] and mouse brain capillary endothelial cells [13]. In a mouse model of experimental autoimmune encephalomyelitis and in human tissue with glioblastoma multiforme, both characterized by compromised integrity of the BBB, selective loss of Cldn3 has been demonstrated at the protein level. It was suggested that Cldn3 is a key component that determines the permeability of BBB endothelial TJs in vivo [49].

TJ mRNA expression analyses have been published from isolated or cultured rodent brain endothelial cells which are comparable to the primary mouse capillary endothelial cells studied here, but these studies do not reflect the in vivo situation. There is broad consensus that Cldn5 is the dominant Cldn species (> 80% of Cldn transcripts) [13, 14, 16, 54]. In addition, most investigators consider that Cldns 3, 9, 10, 11, 12, 15, 19 and 22 are expressed, which is in concordance with our data obtained from laser-dissected mouse capillaries for the underlined transcripts. Nevertheless, there is considerable quantitative variation between the reports, most likely because of very different experimental conditions and the diverse species investigated. Several Cldns were not investigated in either study; especially Cldns 24–27—which have more recently been identified as members of the claudin family [4].

The most probable reason for the limited number of abundant TJ proteins in vitro is that the neurovascular environment does not maintain barrier properties in vitro [2], which leads to down-regulation of all TJ proteins, except Cldn5 and Ocln. Consequently, most in vitro studies mainly address these two proteins and neglect the many others which are worth being considered, as demonstrated by the data presented here. The interdependence between TJ proteins also influences their protein levels seen in bEND.3 cells: knockdown of Cldn5 results in down-regulation of Cldn15 and in strong up-regulation of Cldn1—which could be a further explanation of why Cldn5 knock-out mice retain TJs [12].

Pathological conditions, such as stroke and hypoxia, cause temporary BBB breakdown [47, 55]. We found that Cldn1, -3, and -12, and Ocln are down-regulated early after transient focal cerebral ischemia, while Cldn5 and -25 are up-regulated. The decrease in Ocln mRNA confirms earlier data obtained in different models [25, 56]; but information on the effects of ischemia on transcripts of Cldn12 and -25 is lacking. The up-regulation of Cldn5 is in accordance with the concomitant increase in cadherin-5, which has been demonstrated to sequester β-catenin at the membrane, thereby preventing its translocation to the nucleus [18]. In parallel, loss of Cldn1 and -3 occurs: the transcriptional regulation of their expression in mice has been shown to be dependent on nuclear β-catenin signaling [57]. At the protein level, cross-regulation of Cldn1 and -5 has been described for the cerebellum after global cerebral ischemia/reperfusion (4 h) of the ovine fetus [58].

The mRNA data of Ocln, and Cldn1, -4, -5, -11, -12, and -25 correspond to total protein values as calculated by a new epitope dilution assay. Literature data on the solubilization of TJ proteins [59, 60] suggested that it is necessary to consider both the TX-100-soluble and -insoluble fractions for quantification of the protein levels. Immunohistochemistry of brain slices demonstrates that the above-mentioned proteins (exception, Cldn1), but also Cldn3 and -20, co-localize to the general junction marker Zo1 [61] which, in turn, associates with the TJ-specific marker Ocln [2]. The co-localizations demonstrate the relevance of these Cldns for BBB TJs. As these proteins are expressed in considerable amounts in mouse and human in vivo, it is concluded that they make a significant contribution to the BBB.

Cldn1 is in principle a tightening protein located in TJs of different organs and is clearly detectable in the endothelial cytosol (as also reported earlier [62]), so that the above considerations of mRNA and protein levels cannot be unreservedly transferred to TJ function. Its intracellular localization points to another role and has been correlated with metastatic capacity of human osteosarcoma cells [63] or, on the basis of data from patient biopsies, with increased motility of melanoma cells and progression of melanoma [64, 65]. Thus, one may speculate that an additional function of Cldn1 at the BBB could be related to proliferation and/or migration [66].

We have clearly demonstrated that Cldn11 is present in the TJs of mouse and human BBB. So far, brain Cldn11 protein has been identified in oligodendrocytes [46], in choroid plexus epithelial cells [67] and, very recently, in brain capillaries, blood–spinal cord barrier and blood–arachnoid barrier [17]. We also found Cldn11 mRNA expressed in amounts similar to those of Cldn5 in microdissected brain capillaries originating from 8-µm brain slices. Cldn11 mediates electrical insulation around axons via myelin sheets formed by oligodendrocytes [68] and exerts a tightening function [69]—as confirmed by TER measurements. Its deficiency results in neurological defects in mice [68, 70]. By immunohistochemistry, we found Cldn11 localized both in close proximity to neurons and enriched in capillaries identified by endothelial marker staining; in addition, it co-localized to Zo1. Consequently, Cldn11 and Cldn5 are assumed to act synergistically in native brain capillaries, where they could supplement each other in paracellular tightening. However, in contrast to other authors [17], we do not find a direct interaction of Cldn11 with Cldn5, and there is no indication of interactions between Cldn11 and TAMPs [5] or with other Cldns identified at the BBB. This lack of heterophilic

interaction is very unusual for tightening Cldns and is attributed to the extreme high homophilic association capacity—which is many times higher than for Cldn5 [5, 6]. The strong self-association is related to the low membrane mobility and to the tendency of Cldn11 to polymerize without involvement of other Cldns. The intermittent membrane localization is also reflected by electron microscopic freeze-fracture replicas exhibiting predominantly discontinuous particle lines in TJ strands from brain sections [70] or endothelial cell cultures [71]. On the other hand, Ocln improves the parallelism of P-face-associated Cldn11 TJ strands. Interestingly, transfection of Ocln alone was reported to give rise to poorly developed TJ strands in freeze-fracture replicas [72] while co-transfection with Cldn11 results in large fields of parallel P-face-associated strands. This finding suggests that Ocln may be involved in organizing Cldn11-positive TJs. Interdependence of these two TJ proteins was also found in earlier experiments demonstrating that the knock-down of Ocln in Sertoli cells partially redistributes Cldn11, thus opening the blood–testis barrier [52].

We also demonstrated for the first time that Cldn25 is a novel protein at the BBB. Within the brain, its capillary level is in the range of those of Cldn5, -11 and -12. Likewise, Cldn25 is highly abundant in in vitro systems with similar expression levels to Cldn12 or Ocln. Although Cldn25 alone is unable to generate TJ strands, its knock-down in brain endothelial cells leads to a less accentuated strand network at the extracellular fracture face predominantly formed by Cldn5 [43]. Since Cldn25 *trans*-interacts with Ocln, but not with the other Cldns tested, we assume that it contributes indirectly to TJ formation. Ocln associates with many other TJ proteins [31] and may regulate barrier function under normal [73] and pathological [31] conditions. Preliminary measurements provide hints that the C-terminus of Cldn25 directly binds to Zo1, thus recruiting Ocln and further TJ proteins. In addition, Cldn25 shares similarities with Cldn12. We demonstrate that Cldn25 and -12 are localized within the junctions of cerebral microvessels, together with other TJ proteins in vivo. Both are highly abundant and incapable of forming TJ strands alone. Moreover, there are no changes in BBB permeability, either after Cldn12 knock-out (manuscript in preparation) or after Cldn25 knock-down. In conclusion, Cldn25 is a TJ protein that is highly expressed at the BBB and is capable of modulating the TJ strand network.

In vitro models are often used to evaluate BBB permeability and integrity after drug treatment [74] or pathological events [2], although the corresponding permeation coefficients are much lower than in vivo [53]. We find that Cldn5 is greatly overestimated in cell and capillary preparations compared to mouse brain, where the pattern of TJ proteins is more complex and much more balanced. Consequently, in vitro systems can analyze Cldn5 almost separately from other TJ proteins; however, the rudimentary tetraspanning TJ protein equipment is unfavorable, not only with respect to paracellular barrier permeability, but also for studying signaling processes at the BBB or the effects of pathological conditions. Our study demonstrates that the entire and intact TJ complex can only be studied in in vivo models or, at least, in models closely related to the in vivo situation.

Acknowledgements The authors wish to thank Michael Krauss (FMP Berlin) for help in lentiviral preparation, Susanne Müller (Charité Universitätsmedizin Berlin, Dept. Experimental Neurology) for help in MRI experiments and Ria Knittel (University Hospital, Tübingen, Dept. Pathology and Neuropathology) for skillful assistance with the freeze-fracture technology.

References

1. Krause G, Winkler L, Mueller SL, Haseloff RF, Piontek J, Blasig IE (2008) Structure and function of claudins. Biochim Biophys Acta 1778(3):631–645. https://doi.org/10.1016/j.bbamem.2007.10.018
2. Haseloff RF, Dithmer S, Winkler L, Wolburg H, Blasig IE (2015) Transmembrane proteins of the tight junctions at the blood–brain barrier: structural and functional aspects. Semin Cell Dev Biol 38:16–25. https://doi.org/10.1016/j.semcdb.2014.11.004
3. Maher GJ, Hilton EN, Urquhart JE, Davidson AE, Spencer HL, Black GC, Manson FD (2011) The cataract-associated protein TMEM114, and TMEM235, are glycosylated transmembrane proteins that are distinct from claudin family members. FEBS Lett 585(14):2187–2192. https://doi.org/10.1016/j.febslet.2011.05.060
4. Mineta K, Yamamoto Y, Yamazaki Y, Tanaka H, Tada Y, Saito K, Tamura A, Igarashi M, Endo T, Takeuchi K, Tsukita S (2011) Predicted expansion of the claudin multigene family. FEBS Lett 585(4):606–612. https://doi.org/10.1016/j.febslet.2011.01.028
5. Cording J, Berg J, Kading N, Bellmann C, Tscheik C, Westphal JK, Milatz S, Gunzel D, Wolburg H, Piontek J, Huber O, Blasig IE (2013) In tight junctions, claudins regulate the interactions between occludin, tricellulin and marvelD3, which, inversely, modulate claudin oligomerization. J Cell Sci 126(Pt 2):554–564. https://doi.org/10.1242/jcs.114306
6. Piontek J, Fritzsche S, Cording J, Richter S, Hartwig J, Walter M, Yu D, Turner JR, Gehring C, Rahn HP, Wolburg H, Blasig IE (2011) Elucidating the principles of the molecular organization of heteropolymeric tight junction strands. Cell Mol Life Sci 68(23):3903–3918. https://doi.org/10.1007/s00018-011-0680-z
7. Gunzel D, Yu AS (2013) Claudins and the modulation of tight junction permeability. Physiol Rev 93(2):525–569. https://doi.org/10.1152/physrev.00019.2012
8. Capaldo CT, Nusrat A (2015) Claudin switching: physiological plasticity of the tight junction. Semin Cell Dev Biol 42:22–29. https://doi.org/10.1016/j.semcdb.2015.04.003
9. Gupta IR, Ryan AK (2010) Claudins: unlocking the code to tight junction function during embryogenesis and in disease. Clin Genet 77(4):314–325. https://doi.org/10.1111/j.1399-0004.2010.01397.x
10. Abbott NJ, Patabendige AA, Dolman DE, Yusof SR, Begley DJ (2010) Structure and function of the blood–brain barrier. Neurobiol Dis 37(1):13–25. https://doi.org/10.1016/j.nbd.2009.07.030
11. Ohtsuki S, Sato S, Yamaguchi H, Kamoi M, Asashima T, Terasaki T (2007) Exogenous expression of claudin-5 induces barrier properties in cultured rat brain capillary endothelial cells. J Cell Physiol 210(1):81–86. https://doi.org/10.1002/jcp.20823

12. Nitta T, Hata M, Gotoh S, Seo Y, Sasaki H, Hashimoto N, Furuse M, Tsukita S (2003) Size-selective loosening of the blood–brain barrier in claudin-5-deficient mice. J Cell Biol 161(3):653–660. https://doi.org/10.1083/jcb.200302070
13. Ohtsuki S, Yamaguchi H, Katsukura Y, Asashima T, Terasaki T (2008) mRNA expression levels of tight junction protein genes in mouse brain capillary endothelial cells highly purified by magnetic cell sorting. J Neurochem 104(1):147–154. https://doi.org/10.1111/j.1471-4159.2007.05008.x
14. Daneman R, Zhou L, Agalliu D, Cahoy JD, Kaushal A, Barres BA (2010) The mouse blood–brain barrier transcriptome: a new resource for understanding the development and function of brain endothelial cells. PLoS One 5(10):e13741. https://doi.org/10.1371/journal.pone.0013741
15. Kooij G, Kopplin K, Blasig R, Stuiver M, Koning N, Goverse G, van der Pol SM, van Het Hof B, Gollasch M, Drexhage JA, Reijerkerk A, Meij IC, Mebius R, Willnow TE, Muller D, Blasig IE, de Vries HE (2014) Disturbed function of the blood–cerebrospinal fluid barrier aggravates neuro-inflammation. Acta Neuropathol 128(2):267–277. https://doi.org/10.1007/s00401-013-1227-1
16. Bocsik A, Walter FR, Gyebrovszki A, Fulop L, Blasig I, Dabrowski S, Otvos F, Toth A, Rakhely G, Veszelka S, Vastag M, Szabo-Revesz P, Deli MA (2016) Reversible opening of intercellular junctions of intestinal epithelial and brain endothelial cells with tight junction modulator peptides. J Pharm Sci 105(2):754–765. https://doi.org/10.1016/j.xphs.2015.11.018
17. Uchida Y, Sumiya T, Tachikawa M, Yamakawa T, Murata S, Yagi Y, Sato K, Stephan A, Ito K, Ohtsuki S, Couraud PO, Suzuki T, Terasaki T (2018) Involvement of claudin-11 in disruption of blood–brain, –spinal cord, and –arachnoid barriers in multiple sclerosis. Mol Neurobiol. https://doi.org/10.1007/s12035-018-1207-5
18. Taddei A, Giampietro C, Conti A, Orsenigo F, Breviario F, Pirazzoli V, Potente M, Daly C, Dimmeler S, Dejana E (2008) Endothelial adherens junctions control tight junctions by VE-cadherin-mediated upregulation of claudin-5. Nat Cell Biol 10(8):923–934. https://doi.org/10.1038/ncb1752
19. Huang J, Li J, Qu Y, Zhang J, Zhang L, Chen X, Liu B, Zhu Z (2014) The expression of claudin 1 correlates with beta-catenin and is a prognostic factor of poor outcome in gastric cancer. Int J Oncol 44(4):1293–1301. https://doi.org/10.3892/ijo.2014.2298
20. Liebner S, Corada M, Bangsow T, Babbage J, Taddei A, Czupalla CJ, Reis M, Felici A, Wolburg H, Fruttiger M, Taketo MM, von Melchner H, Plate KH, Gerhardt H, Dejana E (2008) Wnt/beta-catenin signaling controls development of the blood–brain barrier. J Cell Biol 183(3):409–417. https://doi.org/10.1083/jcb.200806024
21. Dorfel MJ, Huber O (2012) Modulation of tight junction structure and function by kinases and phosphatases targeting occludin. J Biomed Biotechnol 2012:807356. https://doi.org/10.1155/2012/807356
22. Titchenell PM, Lin CM, Keil JM, Sundstrom JM, Smith CD, Antonetti DA (2012) Novel atypical PKC inhibitors prevent vascular endothelial growth factor-induced blood–retinal barrier dysfunction. Biochem J 446(3):455–467. https://doi.org/10.1042/BJ20111961
23. Murakami T, Frey T, Lin CM, Antonetti DA (2012) Protein kinase C beta phosphorylates occludin regulating tight junction trafficking in vascular endothelial growth factor-induced permeability in vivo. Diabetes 61(6):1573–1583. https://doi.org/10.2337/db11-1367
24. Daneman R, Prat A (2015) The blood–brain barrier. Cold Spring Harb Perspect Biol 7(1):a020412. https://doi.org/10.1101/cshperspect.a020412
25. Yang Y, Estrada EY, Thompson JF, Liu W, Rosenberg GA (2007) Matrix metalloproteinase-mediated disruption of tight junction proteins in cerebral vessels is reversed by synthetic matrix metalloproteinase inhibitor in focal ischemia in rat. J Cereb Blood Flow Metab 27(4):697–709. https://doi.org/10.1038/sj.jcbfm.9600375
26. Teng F, Beray-Berthat V, Coqueran B, Lesbats C, Kuntz M, Palmier B, Garraud M, Bedfert C, Slane N, Berezowski V, Szeremeta F, Hachani J, Scherman D, Plotkine M, Doan BT, Marchand-Leroux C, Margaill I (2013) Prevention of rt-PA induced blood–brain barrier component degradation by the poly(ADP-ribose)polymerase inhibitor PJ34 after ischemic stroke in mice. Exp Neurol 248:416–428. https://doi.org/10.1016/j.expneurol.2013.07.007
27. Zhang H, Ren C, Gao X, Takahashi T, Sapolsky RM, Steinberg GK, Zhao H (2008) Hypothermia blocks beta-catenin degradation after focal ischemia in rats. Brain Res 1198:182–187. https://doi.org/10.1016/j.brainres.2008.01.007
28. Brown RC, Mark KS, Egleton RD, Huber JD, Burroughs AR, Davis TP (2003) Protection against hypoxia-induced increase in blood–brain barrier permeability: role of tight junction proteins and NFkappaB. J Cell Sci 116(Pt 4):693–700. https://doi.org/10.1242/jcs.00264
29. Li L, McBride DW, Doycheva D, Dixon BJ, Krafft PR, Zhang JH, Tang J (2015) G-CSF attenuates neuroinflammation and stabilizes the blood–brain barrier via the PI3K/Akt/GSK-3beta signaling pathway following neonatal hypoxia–ischemia in rats. Exp Neurol 272:135–144. https://doi.org/10.1016/j.expneurol.2014.12.020
30. Bellmann C, Schreivogel S, Gunther R, Dabrowski S, Schumann M, Wolburg H, Blasig IE (2014) Highly conserved cysteines are involved in the oligomerization of occludin-redox dependency of the second extracellular loop. Antioxid Redox Signal 20(6):855–867. https://doi.org/10.1089/ars.2013.5288
31. Cording J, Gunther R, Vigolo E, Tscheik C, Winkler L, Schlattner I, Lorenz D, Haseloff RF, Schmidt-Ott KM, Wolburg H, Blasig IE (2015) Redox regulation of cell contacts by tricellulin and occludin: redox-sensitive cysteine sites in tricellulin regulate both tri- and bicellular junctions in tissue barriers as shown in hypoxia and ischemia. Antioxid Redox Signal 23(13):1035–1049. https://doi.org/10.1089/ars.2014.6162
32. Blasig IE, Bellmann C, Cording J, del Vecchio G, Zwanziger D, Huber O, Haseloff RF (2011) Occludin protein family: oxidative stress and reducing conditions. Antioxid Redox Signal 15(5):1195–1219. https://doi.org/10.1089/ars.2010.3542
33. Castro V, Bertrand L, Luethen M, Dabrowski S, Lombardi J, Morgan L, Sharova N, Stevenson M, Blasig IE, Toborek M (2016) Occludin controls HIV transcription in brain pericytes via regulation of SIRT-1 activation. FASEB J 30(3):1234–1246. https://doi.org/10.1096/fj.15-277673
34. Engel O, Kolodziej S, Dirnagl U, Prinz V (2011) Modeling stroke in mice—middle cerebral artery occlusion with the filament model. J Vis Exp. https://doi.org/10.3791/2423
35. Mojsilovic-Petrovic J, Nesic M, Pen A, Zhang W, Stanimirovic D (2004) Development of rapid staining protocols for laser-capture microdissection of brain vessels from human and rat coupled to gene expression analyses. J Neurosci Methods 133(1–2):39–48. https://doi.org/10.1016/j.jneumeth.2003.09.026
36. Del Vecchio G, Tscheik C, Tenz K, Helms HC, Winkler L, Blasig R, Blasig IE (2012) Sodium caprate transiently opens claudin-5-containing barriers at tight junctions of epithelial and endothelial cells. Mol Pharm 9(9):2523–2533. https://doi.org/10.1021/mp3001414
37. Haseloff RF, Krause E, Bigl M, Mikoteit K, Stanimirovic D, Blasig IE (2006) Differential protein expression in brain capillary endothelial cells induced by hypoxia and posthypoxic reoxygenation. Proteomics 6(6):1803–1809. https://doi.org/10.1002/pmic.200500182
38. Zwanziger D, Staat C, Andjelkovic AV, Blasig IE (2012) Claudin-derived peptides are internalized via specific endocytosis

pathways. Ann N Y Acad Sci 1257:29–37. https://doi.org/10.1111/j.1749-6632.2012.06567.x
39. Untergasser A, Cutcutache I, Koressaar T, Ye J, Faircloth BC, Remm M, Rozen SG (2012) Primer3-new capabilities and interfaces. Nucleic Acids Res 40(15):e115. https://doi.org/10.1093/nar/gks596
40. Schmidt A, Utepbergenov DI, Krause G, Blasig IE (2001) Use of surface plasmon resonance for real-time analysis of the interaction of ZO-1 and occludin. Biochem Biophys Res Commun 288(5):1194–1199. https://doi.org/10.1006/bbrc.2001.5914
41. Blasig IE, Winkler L, Lassowski B, Mueller SL, Zuleger N, Krause E, Krause G, Gast K, Kolbe M, Piontek J (2006) On the self-association potential of transmembrane tight junction proteins. Cell Mol Life Sci 63(4):505–514. https://doi.org/10.1007/s00018-005-5472-x
42. Dabrowski S, Staat C, Zwanziger D, Sauer RS, Bellmann C, Gunther R, Krause E, Haseloff RF, Rittner H, Blasig IE (2015) Redox-sensitive structure and function of the first extracellular loop of the cell–cell contact protein claudin-1: lessons from molecular structure to animals. Antioxid Redox Signal 22(1):1–14. https://doi.org/10.1089/ars.2013.5706
43. Piontek J, Winkler L, Wolburg H, Muller SL, Zuleger N, Piehl C, Wiesner B, Krause G, Blasig IE (2008) Formation of tight junction: determinants of homophilic interaction between classic claudins. FASEB J 22(1):146–158. https://doi.org/10.1096/fj.07-8319com
44. Tiwari-Woodruff S, Beltran-Parrazal L, Charles A, Keck T, Vu T, Bronstein J (2006) K+ channel KV3.1 associates with OSP/claudin-11 and regulates oligodendrocyte development. Am J Physiol Cell Physiol 291(4):C687–C698. https://doi.org/10.1152/ajpcell.00510.2005
45. Bronstein JM, Popper P, Micevych PE, Farber DB (1996) Isolation and characterization of a novel oligodendrocyte-specific protein. Neurology 47(3):772–778. https://doi.org/10.1212/wnl.47.3.772
46. Morita K, Sasaki H, Fujimoto K, Furuse M, Tsukita S (1999) Claudin-11/OSP-based tight junctions of myelin sheaths in brain and sertoli cells in testis. J Cell Biol 145(3):579–588. https://doi.org/10.1083/jcb.200110122
47. Jiao H, Wang Z, Liu Y, Wang P, Xue Y (2011) Specific role of tight junction proteins claudin-5, occludin, and ZO-1 of the blood–brain barrier in a focal cerebral ischemic insult. J Mol Neurosci 44(2):130–139. https://doi.org/10.1007/s12031-011-9496-4
48. Weuste M, Wurm A, Iandiev I, Wiedemann P, Reichenbach A, Bringmann A (2006) HB-EGF: increase in the ischemic rat retina and inhibition of osmotic glial cell swelling. Biochem Biophys Res Commun 347(1):310–318. https://doi.org/10.1016/j.bbrc.2006.06.077
49. Wolburg H, Wolburg-Buchholz K, Kraus J, Rascher-Eggstein G, Liebner S, Hamm S, Duffner F, Grote EH, Risau W, Engelhardt B (2003) Localization of claudin-3 in tight junctions of the blood–brain barrier is selectively lost during experimental autoimmune encephalomyelitis and human glioblastoma multiforme. Acta Neuropathol 105(6):586–592. https://doi.org/10.1007/s00401-003-0688-z
50. Furuse M, Hata M, Furuse K, Yoshida Y, Haratake A, Sugitani Y, Noda T, Kubo A, Tsukita S (2002) Claudin-based tight junctions are crucial for the mammalian epidermal barrier: a lesson from claudin-1-deficient mice. J Cell Biol 156(6):1099–1111. https://doi.org/10.1083/jcb.200110122
51. Nakano Y, Kim SH, Kim HM, Sanneman JD, Zhang Y, Smith RJ, Marcus DC, Wangemann P, Nessler RA, Banfi B (2009) A claudin-9-based ion permeability barrier is essential for hearing. PLoS Genet 5(8):e1000610. https://doi.org/10.1371/journal.pgen.1000610
52. McCabe MJ, Foo CF, Dinger ME, Smooker PM, Stanton PG (2016) Claudin-11 and occludin are major contributors to Sertoli cell tight junction function, in vitro. Asian J Androl 18(4):620–626. https://doi.org/10.4103/1008-682X.163189
53. Pardridge WM, Triguero D, Yang J, Cancilla PA (1990) Comparison of in vitro and in vivo models of drug transcytosis through the blood–brain barrier. J Pharmacol Exp Ther 253(2):884–891
54. Kratzer I, Vasiljevic A, Rey C, Fevre-Montange M, Saunders N, Strazielle N, Ghersi-Egea JF (2012) Complexity and developmental changes in the expression pattern of claudins at the blood–CSF barrier. Histochem Cell Biol 138(6):861–879. https://doi.org/10.1007/s00418-012-1001-9
55. Liu J, Jin X, Liu KJ, Liu W (2012) Matrix metalloproteinase-2-mediated occludin degradation and caveolin-1-mediated claudin-5 redistribution contribute to blood–brain barrier damage in early ischemic stroke stage. J Neurosci 32(9):3044–3057. https://doi.org/10.1523/JNEUROSCI.6409-11.2012
56. Neuhaus W, Gaiser F, Mahringer A, Franz J, Riethmuller C, Forster C (2014) The pivotal role of astrocytes in an in vitro stroke model of the blood–brain barrier. Front Cell Neurosci 8:78. https://doi.org/10.3389/fncel.2014.00352
57. Tran KA, Zhang XM, Predescu D, Huang XJ, Machado RF, Gothert JR, Malik AB, Valyi-Nagy T, Zhao YY (2016) Endothelial beta-catenin signaling is required for maintaining adult blood–brain barrier integrity and central nervous system homeostasis. Circulation 133(2):177–186. https://doi.org/10.1161/circulationaha.115.015982
58. Chen X, Threlkeld SW, Cummings EE, Juan I, Makeyev O, Besio WG, Gaitanis J, Banks WA, Sadowska GB, Stonestreet BS (2012) Ischemia–reperfusion impairs blood–brain barrier function and alters tight junction protein expression in the ovine fetus. Neuroscience 226:89–100. https://doi.org/10.1016/j.neuroscience.2012.08.043
59. Nusrat A, Parkos CA, Verkade P, Foley CS, Liang TW, Innis-Whitehouse W, Eastburn KK, Madara JL (2000) Tight junctions are membrane microdomains. J Cell Sci 113(10):1771–1781
60. Lynch RD, Francis SA, McCarthy KM, Casas E, Thiele C, Schneeberger EE (2007) Cholesterol depletion alters detergent-specific solubility profiles of selected tight junction proteins and the phosphorylation of occludin. Exp Cell Res 313(12):2597–2610. https://doi.org/10.1016/j.yexcr.2007.05.009
61. Gonzalez-Mariscal L, Quiros M, Diaz-Coranguez M (2011) ZO proteins and redox-dependent processes. Antioxid Redox Signal 15(5):1235–1253. https://doi.org/10.1089/ars.2011.3913
62. Morcos Y, Hosie MJ, Bauer HC, Chan-Ling T (2001) Immunolocalization of occludin and claudin-1 to tight junctions in intact CNS vessels of mammalian retina. J Neurocytol 30(2):107–123. https://doi.org/10.1023/A:1011982906125
63. Jian Y, Chen C, Li B, Tian X (2015) Delocalized claudin-1 promotes metastasis of human osteosarcoma cells. Biochem Biophys Res Commun 466(3):356–361. https://doi.org/10.1016/j.bbrc.2015.09.028
64. French AD, Fiori JL, Camilli TC, Leotlela PD, O'Connell MP, Frank BP, Subaran S, Indig FE, Taub DD, Weeraratna AT (2009) PKC and PKA phosphorylation affect the subcellular localization of claudin-1 in melanoma cells. Int J Med Sci 6(2):93–101. https://doi.org/10.7150/ijms.6.93
65. Leotlela PD, Wade MS, Duray PH, Rhode MJ, Brown HF, Rosenthal DT, Dissanayake SK, Earley R, Indig FE, Nickoloff BJ, Taub DD, Kallioniemi OP, Meltzer P, Morin PJ, Weeraratna AT (2007) Claudin-1 overexpression in melanoma is regulated by PKC and contributes to melanoma cell motility. Oncogene 26(26):3846–3856. https://doi.org/10.1038/sj.onc.1210155
66. Karnati HK, Panigrahi M, Shaik NA, Greig NH, Bagadi SA, Kamal MA, Kapalavayi N (2014) Down regulated expression of claudin-1 and claudin-5 and up regulation of beta-catenin: association with human glioma progression. CNS Neurol Disord Drug

Targets 13(8):1413–1426. https://doi.org/10.2174/1871527313666141023121550
67. Wolburg H, Wolburg-Buchholz K, Liebner S, Engelhardt B (2001) Claudin-1, claudin-2 and claudin-11 are present in tight junctions of choroid plexus epithelium of the mouse. Neurosci Lett 307(2):77–80. https://doi.org/10.1016/s0304-3940(01)01927-9
68. Gow A, Devaux J (2008) A model of tight junction function in central nervous system myelinated axons. Neuron Glia Biol 4(4):307–317. https://doi.org/10.1017/S1740925X09990391
69. Denninger AR, Breglio A, Maheras KJ, LeDuc G, Cristiglio V, Deme B, Gow A, Kirschner DA (2015) Claudin-11 tight junctions in myelin are a barrier to diffusion and lack strong adhesive properties. Biophys J 109(7):1387–1397. https://doi.org/10.1016/j.bpj.2015.08.012
70. Gow A, Southwood CM, Li JS, Pariali M, Riordan GP, Brodie SE, Danias J, Bronstein JM, Kachar B, Lazzarini RA (1999) CNS myelin and sertoli cell tight junction strands are absent in Osp/claudin-11 null mice. Cell 99(6):649–659. https://doi.org/10.1016/S0092-8674(00)81553-6
71. Hulper P, Veszelka S, Walter FR, Wolburg H, Fallier-Becker P, Piontek J, Blasig IE, Lakomek M, Kugler W, Deli MA (2013) Acute effects of short-chain alkylglycerols on blood–brain barrier properties of cultured brain endothelial cells. Br J Pharmacol 169(7):1561–1573. https://doi.org/10.1111/bph.12218
72. Furuse M, Sasaki H, Fujimoto K, Tsukita S (1998) A single gene product, claudin-1 or -2, reconstitutes tight junction strands and recruits occludin in fibroblasts. J Cell Biol 143(2):391–401. https://doi.org/10.1083/jcb.143.2.391
73. Dorfel MJ, Westphal JK, Bellmann C, Krug SM, Cording J, Mittag S, Tauber R, Fromm M, Blasig IE, Huber O (2013) CK2-dependent phosphorylation of occludin regulates the interaction with ZO-proteins and tight junction integrity. Cell Commun Signal 11(1):40. https://doi.org/10.1186/1478-811X-11-40
74. Tscheik C, Blasig IE, Winkler L (2013) Trends in drug delivery through tissue barriers containing tight junctions. Tissue Barriers 1(2):e24565. https://doi.org/10.4161/tisb.24565